Journal of Nuclear Materials 408 (2011) 257–271

Contents lists available at ScienceDirect

Journal of Nuclear Materials

journal homepage: www.elsevier.com/locate/jnucmat

Ag diffusion in cubic silicon carbide

David Shrader [a], Sarah M. Khalil [a], Tyler Gerczak [a], Todd R. Allen [b], Andrew J. Heim [c], Izabela Szlufarska [a,c,*], Dane Morgan [a,c,*]

[a] Materials Science Program, University of Wisconsin–Madison, Madison, WI 53705, USA
[b] Nuclear Engineering and Engineering Physics, University of Wisconsin–Madison, Madison, WI 53706, USA
[c] Materials Science and Engineering Department, University of Wisconsin–Madison, Madison, WI 53706, USA

ARTICLE INFO

Article history:
Received 11 June 2010
Accepted 7 October 2010
Available online 26 November 2010

ABSTRACT

The diffusion of Ag impurities in bulk 3C–SiC is studied using *ab initio* methods based on density functional theory. This work is motivated by the desire to reduce transport of radioactive Ag isotopes through the SiC boundary layer in the Tristructural-Isotropic (TRISO) fuel pellet, which is a significant concern for the Very High Temperature Reactor (VHTR) nuclear reactor concept. The structure and stability of charged Ag and Ag-vacancy clusters in SiC are calculated. Relevant intrinsic SiC defect energies are also determined. The most stable state for the Ag impurity in SiC is found to be a Ag atom substituting on the Si sub-lattice and bound to a C vacancy. Bulk diffusion coefficients are estimated for different impurity states and values are all found to have very high activation energy. The impurity state with the lowest activation energy for diffusion is found to be the Ag interstitial, with an activation energy of approximately 7.9 eV. The high activation energies for Ag diffusion in bulk 3C–SiC cause Ag transport to be very slow in the bulk and suggests that observed Ag transport in this material is due to an alternative mechanism (e.g., grain boundary diffusion).

1. Introduction

Tristructural-Isotropic (TRISO)-coated fuel particles are used in high temperature gas cooled reactors as these particles are designed to stay intact and retain fission products during operation [1]. Considered from the inside outward, individual fuel particles consist of a fuel kernel, usually UO_2 (but can also be UCO), a porous graphite buffer layer, a layer of pyrocarbon, a silicon carbide (SiC) layer, and another pyrocarbon layer [1]. Over ten thousand TRISO particles are then packed into a graphite matrix, which takes the form of a pebble or a rod. The SiC layer provides structural support and it serves as the primary fission product barrier for the fuel. While TRISO coatings are effective in retaining gaseous fission products, a number of experiments have reported an undesired release of Ag from these particles under the high temperatures that might occur during normal and accident conditions [1,2]. Such release could result in deposition of Ag within the reactor, creating significant maintenance and safety concerns. In particular, the deposition of radioactive ^{110m}Ag within the system is a primary concern for worker safety.

In order to achieve a reduction of Ag release from TRISO particles, it is important to first establish the fundamental mechanisms by which Ag is transported through SiC. To understand possible mechanisms we begin by summarizing the existing measurements and explanations of Ag diffusion in SiC. Diffusion coefficients for Ag in SiC have been determined based on at least three methods. The first method fits the overall integrated Ag release from a batch of TRISO fuel particles to a simple diffusion model in order to extract an effective diffusion constant [3–6]. In these experiments TRISO-coated fuel particles are first irradiated to burn the fuel, then annealed at high temperature and the amount of fission product release is measured. Effective diffusion coefficients for each layer are estimated by simulating Fickian diffusion through the TRISO coating and by adjusting the diffusion coefficients to match the experimental fission product release [6]. The second method measures Ag diffusion through use of ion-implanted cubic (3C) SiC samples [7,8]. Such experiments are in some ways more straightforward to interpret than the integral release measurements performed on TRISO particles as only SiC and Ag are involved. The third method for measuring Ag diffusion uses a diffusion couple, which puts Ag in direct contact with SiC and studies diffusion of the Ag into the SiC under different annealing conditions [8,9]. The prefactors and activation energies for diffusion coefficients reported from previous measurements are summarized in Table 1. The first eight values in Table 1 are from integral release measurements or ion implantation where Ag diffusion

* Corresponding authors. Address: Materials Science and Engineering Building, 1509 University Avenue, Madison, WI 53706, USA. Tel.: +1 608 265 5878/5879.
E-mail addresses: izabela@engr.wisc.edu (I. Szlufarska), ddmorgan@wisc.edu (D. Morgan).

0022-3115/$ - see front matter © 2010 Elsevier B.V. All rights reserved.
doi:10.1016/j.jnucmat.2010.10.088

Table 1
Reported diffusion coefficients for Ag in SiC, in the form of $D = D_0 \exp(-Q/k_B T)$. The temperature range shown gives the range of temperature values used to fit the Arrhenius expression for D. The last two values are upper bounds on bulk Ag diffusion coefficients estimated from the absence of observed Ag diffusion. All SiC samples are polycrystalline except for one case Ref. [7] which is labeled "single xtal".

Reference	D_0 (m^2/s)	Q (eV)	Temperature (K)	Measurement
[3]	3.60×10^{-9}	2.23	Not provided	Integral release
[4]	6.76×10^{-9}	2.21	1073–1773	Integral release
[5]	5.00×10^{-10}	1.89	1273–1773	Integral release
[5]	3.50×10^{-10}	2.21	1473–2573	Integral release
[5]	3.60×10^{-9}	2.23	1273–1773	Integral release
[5]	6.80×10^{-11}	1.83	1473–1673	Integral release
[6]	4.50×10^{-9}	2.26	1273–1773	Integral release
[7]	4.30×10^{-12}	2.50	1473–1673	Ion implantation
[7] single xtal	$D < 10^{-21}$ m^2/s		1573	Ion implantation
[8]	$D < 5 \times 10^{-21}$ m^2/s		1773	Ion implantation

profiles was observed. The last two values are from ion-implantation experiments on 3C–SiC samples where no Ag diffusion was detected. The lack of any observed diffusion provides an upper bound on the diffusion coefficients in bulk SiC.

In order to explain the values in Table 1 we now consider possible underlying diffusion mechanisms for Ag through SiC and TRISO particles. These mechanisms include solid phase transport of Ag through SiC bulk and grain boundaries and vapor or surface transport through pores and cracks (potentially with additional contributions from transport through C layers in the full TRISO particles). Each of the three types of experiments mentioned above has advantages and disadvantages for elucidating Ag diffusion mechanisms.

The first type of experiment mentioned above, integral release [3–6] measurements, have the advantage of being extracted from measurements performed on real TRISO particles but have the disadvantage of potentially being dependent on all diffusion mechanisms and therefore difficult to analyze. Variation in integral release diffusion coefficients between similar experiments done with different SiC microstructures (values range from 8.44×10^{-18} to 1.85×10^{-16} m^2/s at 1200 °C) suggests that the SiC microstructure plays a significant role in Ag diffusion and supports the hypothesis that grain boundary transport may be the dominant mechanism of Ag diffusion in SiC [6].

Ion implantation is the second type of experiment mentioned above. Ion implantation studies are able to focus directly on Ag transport through SiC but leave considerable damage during the implantation process which is not prototypic of the damage caused by neutron irradiation. This damage must be annealed out before proper Ag concentration profiles can be obtained. Ion implantation studies done on single-crystal SiC allow the investigation of Ag diffusion in bulk SiC (such diffusion is generally called bulk or volume diffusion), while ion implantation studies done on polycrystalline SiC allow also for the investigation of grain boundary diffusion. Friedland et al. [7] has done both types of ion-implantation experiments and found that Ag diffusion was observed in the polycrystalline samples, but that no diffusion of Ag was observed in the single-crystal experiments. These results again suggest that Ag diffusion in SiC may be dominated by grain boundary transport. However, the values obtained by Friedland et al. are approximately 10^3 times smaller than those obtained from integral release, suggesting other mechanisms may a play a role in the integral release data. In addition, MacLean [8] argues that grain boundary diffusion is not able to account for the spread in reported data as the ranges of Ag diffusion path lengths required to describe all reported data would be very unlikely. Specifically, MacLean points out that, under the assumption of a single effective diffusion coefficient for all types of grain boundaries, path lengths up to 13 times the thickness of the SiC layer would be required to explain the data in terms of changing grain boundary path length alone. In support of this argument, experiments done by MacLean using ion implantation on polycrystalline SiC showed no detectable movement of Ag in SiC, even when the Ag was in contact with SiC grain boundaries.

The last type of experiment is the use of diffusion couples. In addition to the ion implantation studies mentioned above, MacLean has also done diffusion couple experiments with Ag and SiC [8]. Diffusion couple experiments measure Ag penetration into the SiC sample from which diffusion coefficients can be determined and allow us to look at the direct interaction between Ag and SiC. In these experiments, Ag was placed inside a spherical SiC shell and exposed to temperatures above 1050 °C. MacLean observed no Ag penetration into the SiC shell yet noted there was significant mass loss for Ag. MacLean has proposed that vapor transport through mechanical structures (such as cracks or pores) may be the dominant method of Ag transport in SiC.

The above discussion demonstrates that there is significant uncertainty about both the diffusion coefficient and the diffusion mechanisms of Ag in SiC. In order to better understand the diffusion mechanisms of Ag in SiC, we use *ab initio* based modeling of Ag defects and their mobility to determine the nature of the Ag defect structures and the fundamental mechanisms and rates by which these defects diffuse. This work focuses only on Ag diffusion in bulk SiC. While it is expected that this diffusion will be slow [7,8], the investigation will allow us to identify the key energies associated with Ag migration in SiC. Once these energies are understood, they can guide the *ab initio* investigation of more complicated structures such as grain boundaries.

2. Methods

Ab initio calculations were performed using density functional theory (DFT) and the projector-augmented plane-wave (PAW) method [10,11], with the Vienna Ab-initio Simulation Package (VASP) [12–15]. Exchange–correlation was treated in the Generalized Gradient Approximation (GGA), as parameterized by Perdew, Burke, and Ernzerhof (PBE) [16,17]. The PAW potentials were generated with the following valence electronic configurations: 3s2 3p2 for Si, 2s2 sp2 for C, and 5s1 4d10 for Ag. All calculations were spin polarized and almost without exception, all defects exhibited magnetic moments for some of the charge states investigated. Typical moments were less than one, but moments as high as three were observed for Si-site related defects (for example, Si vacancies and Ag on Si substitutionals). The Brillouin zone was sampled by a Monkhorst–Pack k-point mesh of $6 \times 6 \times 6$ for the 8-atom conventional SiC cell, and the Fourier space k-point density was kept as constant as possible for different cells. The energy cutoff was set to 600 eV. Errors in energy convergence with respect to k-points and cutoff was lower than 5 meV/atom. Bulk defect calculations were done in a $2 \times 2 \times 2$ supercell of the conventional cell containing 64 atoms for the undefected SiC system.

The equation for the formation energy of a defect is given by [18,19]:

$$\Delta E_f = E_{\text{def}} - E_{\text{undef}} + \sum_I \Delta n_I (E_I + \gamma_I) + q\left(E_{\text{VBM}} + \left(E_{\text{def}}^{\text{core}} - E_{\text{undef}}^{\text{core}}\right) + \mu_{\text{F}}\right) + E_{\text{MP}} \quad (1)$$

In Eq. (1) E_{def} is the energy of the defected cell, E_{undef} is the energy of the undefected cell, Δn_I is the number of atomic species I in the undefected cell minus the number of the same species in the defected cell, E_I is the energy of atomic species I in its reference state (usually bulk solid or gas), γ_I is the chemical potential of atomic species I relative to its reference state E_I ($\mu_I = E_I + \gamma_I$ is the chemical potential of species I relative to the reference state used to determined E_I), q is the number of electrons transferred to/from the electronic

reservoir (negative for moving electrons from the reservoir into the cell, positive for moving electrons from the cell to the reservoir), E_{VBM} is the energy of the valence band maximum in the undefected cell (we assume the electron comes from/goes to a location far from the defect), and μ_F is the chemical potential of the electrons (Fermi level) relative to E_{VBM}. The chemical potential of the electrons can vary from the valence band maximum ($\mu_F = 0$; p-type doping conditions) to the conduction band minimum (μ_F = energy of the band gap, E_{gap}; n-type doping conditions).

Energy E_I will be determined using *ab initio* calculations. The term $(E^{core}_{def} - E^{core}_{undef})$ in Eq. (1) is an electronic potential shift term [18,20], which is necessary to align the energy that would be obtained for the valence band maximum of the defected cell if one could measure it far from the defect (where the impact of the defect would be negligible) with the energy of the undefected cell valence band maximum. The shift assures that the Fermi level is defined with respect to the same valence band level in both the undefected and defected cells. In this work we determine the shift of band structures by aligning low energy electronic levels (core-like levels) in the density of states (DOS), following the approach of Bockstedte et al. [21]. E^{core}_{def} represents the core-like electronic level in the defected cell and E^{core}_{undef} is the core-like electronic level in the undefected cell. E_{MP} is the correction proposed by Makov and Payne [22] to correct for spurious interactions between periodic images of charged defects in periodic systems. Both the monopole–monopole and monopole–quadrupole corrections are used.

There is some uncertainty in estimating the corrections just mentioned. The electronic alignment correction was done by aligning electronic states near the bottom of the average DOS of the defected cell with that of the pure, defect-free cell. The shift determined by this alignment of low energy levels was consistent with a shift needed to bring the projected density of states at an atom far from the defect into alignment with the projected density of states of an atom of the same species in the pure cell. The use of density of state calculations to determine the electronic alignment has been done in Ref. [21]. An alternative method of calculating the electronic alignment is to use electrostatic potentials at sites far from the defect. The difference between the electrostatic potentials of an atom far from the defect in the defected cell and the pure cell is taken to be the electronic shift. This method has been used by Refs. [20,23]. However, for our calculations in SiC the shift predicted by the difference of electrostatic potential at an atom far from the defect did not equal the shift predicted by an analysis of the projected density of states at the same atom. The differences in the predicted shifts between the two methods could be as large as 200 meV. We choose to use the average density of states method as it predicts a shift that consistently aligns the projected density of states of individual atoms far from the defect to that of the pure cell. We estimate an error in the electronic alignment of around 100 meV based on the discrepancy between the two methods just described. The error in formation energies may be larger than this because the correction is multiplied by the charge of the defect. For example, if the shift had an error of 100 meV and a defect has a charge of 3− ($q = -3$ in Eq. (1)), the defect would have an error of 300 meV/defect.

Similar to the uncertainties is determining the band shift, certain approximations are used in obtaining the monopole–quadrupole term in the correction proposed by Makov and Payne. The uncertainty in this term comes primarily from the step of calculating the defect-induced quadrupole moment within the defected cell. In order to calculate the proper quadrupole moment, the center of the charge distribution associated with the charged defect must be determined [24]. It was found that using high-symmetry points of the bulk structure (such as C and Si sites and tetrahedrally coordinated interstitial sites) as the center of the charge distribution yielded the expected magnitude for the correction (<0.5 eV). The final values used in our calculations were found by selecting the lowest defect-induced quadrupole moment of the defected cell from a set of quadrupole moment calculations where the center of the charge distribution was considered at a series of typically 3–4 different high-symmetry points. The procedure used to find the center of the charge distribution is not comprehensive and therefore may miss the true center of the charge distribution in complex defect clusters where more than one atomic site is involved. This possibility introduces a certain amount of uncertainty in the monopole–quadrupole correction. One option to avoid the quadrupole term errors is to include only monopole–monopole terms, but such an approach has been shown to yield a significant overcorrection of the electrostatic errors in some systems [20]. The error from the choice of charge distribution center in the monopole–quadrupole correction term is estimated to be about 100 meV in a typical defect calculation. This estimate is based on the spread in values we see for different choices of the charge distribution center. Combining all these effects suggests that energies for charged defects can easily have errors of up to 0.5 eV/defect, and accuracy below 100 meV/defect is probably not reasonable to expect. The calculation of diffusion coefficients typically involves the addition of a few of the key energies, each of which may have ~0.5 eV/defect error associated with them. Therefore, it is expected that activation energies in calculated diffusion coefficients will have a comparable error, possibly as high as ~1 eV. Despite these errors we believe the qualitative results of this work are robust. The central results of this work are identification of the most stable defect states of Ag in SiC and their mechanisms and qualitative magnitudes of diffusion, all of which should be similar even under changes of energies approaching 1 eV. The uncertainties associated with charged defect calculations combined with those associated with other aspects of *ab initio* modeling (e.g., the exchange–correlation function approximations and pseudopotentials), can yield quite different results when different groups calculate energies of the same charged defects. We have used the best methods available that are practical for the large number of energies that must be determined and where possible, we compare our results to previously published studies.

It is important to note that many defect reactions involve exchanging atoms or electrons with an external reservoir, the stability of which is governed by a chemical potential. Therefore, the formation energy of a defect can depend on the chemical potential of Si, C, and electrons. The chemical potential of the electrons has already been discussed above and is given by the Fermi energy. The external chemical potentials of Si and C are interrelated and can be bounded at equilibrium by stability considerations. In particular, the Si and C chemical potentials may not be higher than the values of the bulk phases (graphite and bulk silicon) or these bulk phases would form spontaneously and reduce the chemical potential. Furthermore, in thermodynamic equilibrium, the chemical potentials of Si and C, μ_{Si} and μ_C, are related to the chemical potential of the SiC crystal by $\mu_{SiC} = \mu_{Si} + \mu_C$. These constraints combined provide upper and lower bounds on μ_{Si} and μ_C.

Here we give a quantitative description of the values for μ_{Si} and μ_C which will be used in our calculations of defects. It is assumed that the relevant energies of bulk Si, C and SiC can be described by their *ab initio* calculated zero-temperature energies. We define E_I as the *ab initio* energy of the bulk phase of species I, E_{SiC} as the *ab initio* energy of bulk SiC, and E_f as the *ab initio* formation energy of SiC ($E_f = E_{SiC} - E_{Si} - E_C = -0.44$ eV/FU (FU = formula unit) in our calculations). The constraints of equilibrium can now be shown to give a range of chemical potential values for species I of $E_f < \mu_I < E_I$. The chemical potentials are typically taken for three types of conditions, corresponding to a SiC alloy that has excess Si (Si rich), excess C (C rich), or a balance halfway between these extremes, where the deviation of chemical potential from the bulk

Table 2
External chemical potentials for Si and C that will be used throughout this work.

Case	μ_{Si}	μ_C	γ_{Si}	γ_C
Si rich	E_{Si} = −5.44 eV	$E_{SiC} - E_{Si}$ = −9.65 eV	0	E_f = −0.44 eV
C rich	$E_{SiC} - E_C$ = −5.89	E_C = −9.20 eV	E_f = −0.44 eV	0
$\gamma_{Si} = \gamma_C$	−5.67 eV	−9.43 eV	−0.22 eV	−0.22 eV

phase are equal for both Si and C ($\gamma_{Si} = \gamma_C$, where γ is defined in Eq. (1)). The μ and γ values for these cases are given in Table 2. In the following text, results will be reported for both Si- and C-rich (and in some cases also for $\gamma_{Si} = \gamma_C$) conditions. The Si- and C-rich cases provide the bounds on the formation energy of defects with respect to the Si and C reservoir chemical potential ranges. The chemical potential of Ag is always set to the *ab initio* formation energy of bulk solid phase Ag metal.

In order to model Ag defect energetics in SiC, it is necessary to identify the charge state of the Ag defects. The defect charge state is given by the number of electrons (holes) that are associated with the defect in addition to those obtained in a neutral DFT calculation of the defected cell. These additional electrons (holes) are associated with states in the band gap. Possible charged defect states are identified by adding electrons (holes) into the defected cell until the added charges relax into the conduction (valence) bands, i.e., the additional charges are no longer associated with the defect. The cases where the electrons (holes) do not relax to the conduction (valence) band are the possible charged defect states. The most stable charge state for a given defect is identified as the one that has the lowest energy at the given Fermi energy. In order to determine if an added electron charge $\Delta q = q_2 - q_1$ is relaxing into the conduction band, the quantity $\Delta E/|\Delta q|$ (where $\Delta E = E_f(q_2) - E_f(q_1)$ and $E(q)$ is determined from Eq. (1) with $\mu_F = 0$) is calculated and compared to the *ab initio* band gap. If $\Delta E/|\Delta q| > E_{gap}$ then the electron is assumed to have relaxed into the conduction band. In order to determine if a hole is relaxing into the valence band, the inequality $\Delta E/|\Delta q| > 0$ is tested, where satisfying the inequality corresponds to a hole relaxing into the valence band. Note that Δq is negative for adding an electron and positive for adding a hole.

One complicating factor that occurs in applying the above test for electrons being added to the cell is that the charge states of a defect correspond to integral charges, i.e., Δq is an integer. However, $\Delta E/|\Delta q|$ is not constant with the magnitude of Δq. For example, for pure SiC, adding $\Delta q = 0.05$ gives $\Delta E/|\Delta q| = 1.1$ eV, very close to the band gap of 1.07 eV we extract from our density of states. However, adding $\Delta q = 1$ yields $\Delta E/|\Delta q| = 1.65$ eV. The difference is expected as the extra electrons are added into the conduction band and fill empty states, raising the Fermi level and increasing $\Delta E/|\Delta q|$. This result demonstrates that $\Delta E/|\Delta q| > E_{gap}$ could be obtained even when the entire electron does not enter the conduction band. In such a case the above test would identify the electron as relaxing into the conduction band while instead it was perhaps charging the defect. In order to identify cases where such effects occur negative charge states were initially explored with integral values, i.e., using $\Delta q = 1$ between all charge states. If the change in energy going from state $-q$ to $-(q+1)$ gives $\Delta E/(\Delta q = 1) > 1.65$ eV then the electron was assumed to enter the conduction band. If $E_{gap} < \Delta E/|\Delta q| < 1.65$ eV then the fate of the electron is somewhat ambiguous, as it gains too much energy to be in a state in the gap and too little energy to be entering the conduction band. These ambiguous cases are perhaps due to levels that are quite close to the conduction band minimum and hybridize at least partly with the conduction band. In order to treat theses ambiguous cases an additional calculation with $\Delta q = 0.1$ was attempted. If $\Delta E/(\Delta q = 0.1) < E_{gap}$ then the defect was assumed to have a stable charge state $-(q+1)$. A concrete example of where an integral charge addition had to be further investigated occurred for the Si vacancy (V_{Si}) defect. Calculations found that $E\left(V_{Si}^{2-}\right) - E\left(V_{Si}^{1-}\right) = 1.07$ eV, yielding $\Delta E/(\Delta q = 1) \approx E_{gap}$. Thus a further calculation with $\Delta q = 0.1$ ($q = -1.1$) was preformed and yielded $\Delta E/(\Delta q = 0.1) = 0.89$ eV $< E_{gap}$. The latter result suggests that the additional electron is entering a defect state within the gap, and consequently V_{Si}^{2-} was assumed to be a possible charged defect state.

Finally, it should be noted that the computed gap of 1.07 eV is quite far from the experimental value of 2.39 eV for 3C–SiC [25]. The under-estimation of the band gap is a fundamental shortcoming of the DFT formalism. This discrepancy has at least three major implications. The first and most serious implication is that some negatively charged defect states, which should be placed in the gap, may end up outside the gap because the electron relaxes into the unphysically low conduction band. The second implication of the gap error is that defect levels within the gap are likely to be at the wrong energy with respect to the valence band. Therefore, the predicted ionization levels within the gap shown in this work are generally not reliable. There are a number of approximate corrections to this problem (e.g., see discussions Refs. [20,26–29]). It is unclear to what extent these correction schemes will help increase the accuracy of defect and impurity formation energies in SiC, and they have therefore not been used in this work. Instead, the data is presented as calculated, with no band gap correction scheme. It is also possible to use hybrid density functional or DFT-GW approaches to overcome these band gap issues [30–32], but these methods have not been used in this work due to computational limitations.

Finally, the third implication of the gap error is that a choice must be made about which gap to use for the value of the Fermi energy for n-type doping in Eq. (1). Energy values reported in this work for n-type doping conditions assume that electrons come from a conduction band separated from the valence band by the experimental band gap of 2.39 eV. Choosing the experimental gap for determining charge states in DFT calculations is a common practice [21,33].

3. Results

3.1. SiC defect formation energies

In order to model Ag impurity diffusion it is useful to know the intrinsic SiC defect energetics. Although other studies of such defects have been previously reported, there is a large spread in the published data. In order to establish a self-consistent set of data for this work we perform calculations of intrinsic SiC defects with the same methods as those used in our calculations of Ag energetics. Table 3 contains defect formation energies for intrinsic SiC defects and compares them to values found in the literature. Energies for all possible defect charge states that can be formed (i.e., for which the added electrons (holes) do not enter the conduction (valence) band) are given, although only some may be stable over the range of allowed electron chemical potentials. We report values for n-type SiC ($\mu_F = 2.39$ eV in Eq. (1)) as it has been found that as-prepared is generally slightly n-type [34–37], but p-type doping conditions can be obtained by subtracting the charge state (where added electrons correspond to a charge state with a value less than zero) multiplied by the experimental band gap (2.39 eV) from the n-type formation energies. Only the most stable interstitials in the n-type doping limit are reported, which are the Si–Si ⟨1 1 0⟩ and C–C ⟨1 0 0⟩ split dumbbell interstitials. Mixed dumbbells were also investigated but all were mechanically unstable except for the C–Si ⟨1 1 0⟩ dumbbell, which had a formation energy of 7.64 eV for the neutral case. This result for interstitials is consistent with findings reported in Ref. [21]. We report values for the Si-rich, C-rich, and $\gamma_{Si} = \gamma_C$ chemical potentials (see Section 2).

Table 3
Comparison of SiC intrinsic defect formation energies. C-rich, Si-rich, and $\gamma_{Si} = \gamma_C$ refer to reservoir chemical potentials and are described in the text. All literature sources except for [21,33], which are for Si-rich conditions, use $\gamma_{Si} = \gamma_C$ conditions. Energies are given in eV and are for n-type doping conditions.

Defect	This work			[21]	[33]	[38]	[39][a]	[40][a]	[35][b]	[41][b]	[42][b]
	C-rich	Si-rich	$\gamma_{Si} = \gamma_C$								
V_C^{2+}	6.96	6.51	6.73	6.03	5.66						
V_C^{1+}	5.57	5.13	5.35		4.99						
V_C^{0}	4.64	4.19	4.41	3.73	4.30	3.47	2.77	4.8	4.53	4.11	4.50
V_{Si}^{1+}	9.53	9.97	9.75	10.7	10.7						
V_{Si}^{0}	7.19	7.63	7.41	8.33	8.45	7.62	7.79	8.45	8.17	8.01	7.80
V_{Si}^{1-}	5.32	5.76	5.54	6.51	7.46						
V_{Si}^{2-}	4.52	4.97	4.74	5.93	7.01						
C_{Si}^{0}	3.15	4.03	3.59						3.84	4.06	
Si_C^{1+}	6.72	5.84	6.28								
Si_C^{0}	4.45	3.56	4.01						4.56	4.46	
Si–Si $\langle 1\,1\,0\rangle^{+2}$	12.54	12.10	12.32	11.9							
Si–Si $\langle 1\,1\,0\rangle^{+1}$	10.64	10.20	10.42	9.93							
Si–Si $\langle 1\,1\,0\rangle^{0}$	9.20	8.75	8.97	8.56							9.40
C–C $\langle 1\,0\,0\rangle^{+2}$	9.51	9.95	9.73	10.1							
C–C $\langle 1\,0\,0\rangle^{+1}$	7.76	8.20	7.98	8.37							
C–C $\langle 1\,0\,0\rangle^{0}$	6.51	6.95	6.73	6.71						4.53	7.00

[a] As quoted in [38].
[b] As quoted in [43].

There are several points to make in comparing our data and that in the literature. First, in the literature, only the C and Si vacancy defects have been widely calculated, and there is an agreement to within about 0.5 eV among different researchers on the values. Other defect energies have no more than a few sources for comparison, and often vary over many eV's. Our values for the C vacancy are on the higher end of the values reported in the literature. Our values for the Si vacancy are on the lower end of the literature values. However, in both cases we are consistent with previous results, which lend support to the accuracy of our calculations. Our C vacancy does not show the Jahn–Teller distortion that has been found previously by a number of authors Refs. [21,33]. However, our C–C $\langle 1\,0\,0\rangle$ dumbbell interstitial does exhibit the Jahn–Teller distortion described in Ref. [21]. In addition, there is a surprisingly large range of values reported for interstitial defects, making it difficult to assess the accuracy of any of the values. The range of values for interstitials is so great that not even the order of stability of interstitials is agreed upon. We are, however, within the range found by other authors. Some of the differences between charged defect energies reported here and those reported in the literature could be due to our use of GGA for the exchange correlation where literature sources used the local density approximation (LDA). In general we agree with the quite thorough SiC study of Bockstedte, et al. [21] on the most stable charge state of the defects in the n-type doping limit. The one exception is for the C–C $\langle 1\,0\,0\rangle$ split dumbbell, where we predict the most stable charge state to be neutral and Bockstedte, et al. predict a charge state of 1− to be the most stable.

3.2. Ag Defect formation energies

Formation energies for Ag defects are listed in Table 4. As with the intrinsic SiC defects, all possible charge states are shown. For Ag defect clusters the binding energy is also given. The binding energy is the energy change associated with the reaction of combining the isolated point defects in their most stable charge states into the cluster in its most stable charge state. This work has studied Ag interstitial and substitutional defects, including Ag-vacancy defect clusters with up to two vacancies (Ag-vacancy clusters with three vacancies were not considered as the two-vacancy clusters were already less stable than the single vacancy clusters).

Ag formation energies as a function of electron chemical potential are shown in Fig. 1. In the n-type doping limit, Ag prefers to occupy Si lattice sites as opposed the C lattice sites, and prefers a charge state of 3−. However, for p-type the Ag prefers to be on the C site with a charge of 3+. Ag is somewhat larger than Si and much larger than C (covalent radii are 1.59 Å (Ag), 1.20 Å (Si), 0.68 Å (C)[44]), which is consistent with positive charge states (which create a smaller Ag atom) preferring C sites and negative charge states (which create a larger Ag atom) preferring Si sites. The ionicity of SiC (the covalent bond is 10% ionic due to the different electronegativities of Si and C [44,45]) may also play a role, as the ability of the Ag on Si substitutional defect to supply missing electrons for the surrounding C atoms makes it energetically favorable for the Ag to form a negative charge state. As discussed in Section 2, the possible charge states for Ag defects are determined by finding the bounds past which additional electrons are placed in the conduction band or holes in the valence band. Below we report the stable charge states for each defect, and which charge state is stable in the n-type doping limit. For example, the Ag on Si substitutional can take on charge states of 1+, 0, 1−, 2−, and 3− and will be found with a charge state of 3− in n-type doping conditions. The addition of four electrons to the simulation cell places the extra charge into the conduction band, and the 2+ simulation pulled charge from the valence band. The Ag on C substitutional can take on charge states of 3+, 2+, 1+, and 0 and will be found in the neutral charge state in n-type doping conditions.

We have investigated a number of interstitial configurations, among which only three structures were found to be mechanically stable (i.e., other initial interstitial configurations relaxed to one of these three structures): Ag_{TC}, Ag_{TSi}, and Ag–Si $\langle 1\,1\,0\rangle$ dumbbell. Ag_{TC} is a configuration where an interstitial Ag is tetragonally coordinated between four C atoms. Ag_{TSi} is an analogous configuration with Ag surrounded by four Si atoms. Ag–Si $\langle 1\,1\,0\rangle$ is a dumbbell configuration where Ag shares a Si lattice site with another Si atom and the dumbbell is aligned along the $\langle 1\,1\,0\rangle$ direction. We identified possible charge states of Ag_{TC} to be 1+ and 0. Ag_{TSi} has possible charge states of 1+ and 0 and Ag–Si $\langle 1\,1\,0\rangle$ has possible charge states of 2+, 1+, and 0. All of these interstitials will be found in the neutral charge state in n-type doping conditions.

The most stable Ag defect is actually a defect cluster that includes Ag somewhat relaxed off a Si lattice site and bound to a C vacancy. This defect, denoted as Ag_{Si}–V_C, was formed by placing

Table 4
Defect formation energies for Ag defects under n-type doping conditions. Numbers in Binding rows are binding energies for defect clusters relative to the isolated defects making up the cluster. Numbers in bold are the most stable charge state for that defect under n-type doping conditions.

Defect	Charge state							
	4−	3−	2−	1−	0	1+	2+	3+
Ag_{Si}								
Si-rich		**3.71**	4.12	5.05	6.60	8.77		
C-rich		**3.27**	3.68	4.61	6.16	8.33		
Ag_C								
Si-rich					**7.39**	8.10	9.40	11.18
C-rich					**7.83**	8.54	9.84	11.62
Ag_{TC}								
Si-rich					**10.49**	11.17		
C-rich					**10.49**	11.17		
Ag_{TSi}								
Si-rich					**11.38**	12.20		
C-rich					**11.38**	12.20		
Ag–Si ⟨1 1 0⟩								
Si-rich					**10.91**	12.18	14.46	
C-rich					**10.91**	12.18	14.46	
Ag_{Si}–V_{Si}								
Si-rich		**9.99**	10.58	11.80	13.53			
C-rich		**9.10**	9.69	10.91	12.65			
Binding		1.31	1.90	3.12	4.85			
Ag_{Si}–V_C–C_{Si}								
Si-rich				**6.91**	8.56	10.76		
C-rich				**6.03**	7.67	9.88		
Binding				−5.03	−3.38	−1.18		
Ag_C–V_C								
Si-rich						**9.49**	11.19	13.31
C-rich						**10.37**	12.08	14.20
Binding						−2.10	−0.39	1.73
Ag_{Si}–V_C–Si_C								
Si-rich				**5.80**	7.05	8.88		
C-rich				**6.69**	7.93	9.76		
Binding				−5.67	−4.42	−2.59		
Ag_{Si}–V_C								
Si-rich				**3.46**	5.32	7.69		
C-rich				**3.46**	5.32	7.69		
Binding[a]				−4.44	−2.59	−0.21		
Ag_{Si}–$2V_C$								
Si-rich					**6.44**	7.59	10.29	
C-rich					**6.88**	8.03	10.73	
Binding					−5.66	−4.51	−1.81	
Ag_C–$2V_{Si}$								
Si-rich	**7.18**	7.37	8.12	9.39	11.40	13.70		
C-rich	**6.74**	6.93	7.68	8.95	10.96	13.25		
Binding	−10.14	−9.95	−9.20	−7.93	−5.92	−3.26		
Ag_{Si}–V_C–V_{Si}								
Si-rich	**6.65**	6.84	7.55	8.99	10.97	13.40		
C-rich	**6.21**	6.39	7.11	8.54	10.52	12.95		
Binding	−6.22	−6.03	−5.32	−3.88	−1.91	0.53		

[a] To separate into Ag_{Si}^{3-} and V_C^0.

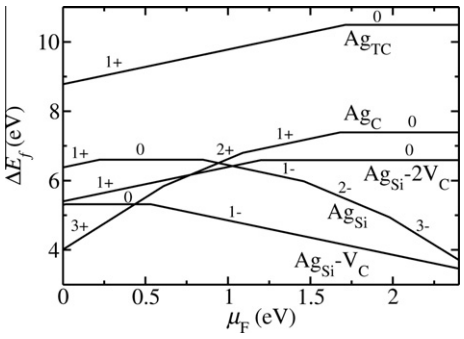

Fig. 1. Ag formation energies as a function of electronic doping level. Energies are for Si-rich conditions. Only the most stable interstitial and two-vacancy clusters are shown. Therefore, all other Ag interstitials are expected to lie above the Ag_{TC} line and all other two-vacancy clusters are expected to lie above the Ag_{Si}–$2V_C$ line.

Ag directly on a Si lattice site and removing one of the nearest-neighbor C atoms as shown in Fig. 2. When the configuration is relaxed, the magnitude of the Ag displacement toward the C vacancy is 37% of the Si–C bond length (1.89 Å) in an ideal 3C–SiC. The possible charge states of the Ag_{Si}–V_C defect are 1+, 0, and 1− and in the n-type doping limit the defect has a charge state of 1−.

A defect closely related to Ag_{Si}–V_C is the cluster of Ag on C next to a Si vacancy (Ag_C–V_{Si}). However, this cluster is not stable and transforms during relaxation to the configuration of Ag_{Si}–V_C. Thus, Ag_{Si}–V_C and Ag_C–V_{Si} relax to equivalent structures, and as the Ag is closer to the Si site, we refer to this structure as Ag_{Si}–V_C.

A defect cluster with Ag near a Si lattice site with two of the four nearest-neighbor C atoms being vacant (Ag_{Si}–$2V_C$) has also been investigated. The unrelaxed structure of this defect is shown in Fig. 3. There are six ways to orient this cluster within the SiC lattice but they are all symmetry equivalent and consequently there exists only one symmetry distinct structure. When the configuration is relaxed, the Ag is displaced 0.59 Å from the ideal Si lattice site

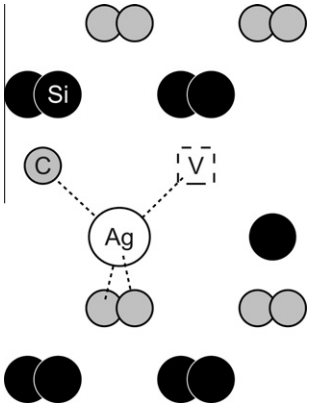

Fig. 2. Schematic picture of the unrelaxed Ag_{Si}–V_C defect complex. Black, grey, and white spheres correspond to Si, C, and Ag atoms, respectively. White squares represent vacancies, in this case on a C site. An antisite defect is denoted with the same symbol as the usual species on the lattice but with a double line boundary (not shown here – see Fig. 5 for an example). These symbols will be used throughout the figures in the paper and have the same meanings as here. Ag resides on a Si lattice site. The four nearest neighbors of the Ag atom are represented by the dotted lines.

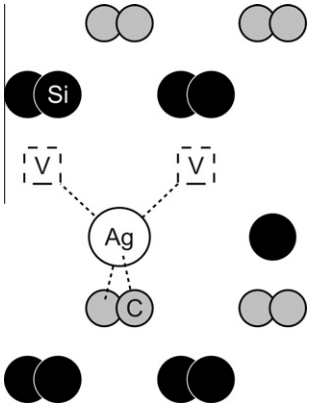

Fig. 3. Schematic picture of the unrelaxed Ag_{Si}–$2V_C$ defect cluster.

toward the center of the bond between the two V_C, slightly favoring one of the vacancies, but the relatively small displacement means the Ag is still clearly associated with the Si site. Possible charge states for this defect are 2+, 1+ and 0, with the most stable charge state in n-type doping conditions being 0. The formation energies for this defect are higher than for the Ag_{Si}–V_C defect cluster. However, the presence of another vacancy may allow lower migration energies than for Ag_{Si}–V_C and therefore the migration mechanisms of this defect will be investigated.

The analogous defect cluster to Ag_{Si}–$2V_C$ with Ag centered on the C site (Ag_C–$2V_{Si}$) is only stable when calculations are constrained to keep the Ag exactly between the two Si vacancy sites. If the Ag is allowed off this symmetry point, the Ag relaxes to fill a Si vacancy to form a Ag_{Si}–V_C configuration, leaving behind an unbound Si vacancy as depicted in Fig. 4. This configuration is denoted as Ag_{Si}–V_C–V_{Si}. Ag_{Si}–V_C–V_{Si} has the same possible charge states as Ag_C–$2V_{Si}$, which are 4−, 3−, 2−, 1−, and 0. The most stable charge state for n-type doping conditions is 4−. For all charge states, Ag_{Si}–V_C–V_{Si} is more stable than Ag_C–$2V_{Si}$ by about half an eV. Therefore, Ag_C–$2V_{Si}$ is an unstable configuration, and diffusion analysis will not be done for this cluster. Instead, diffusion analysis will be carried out for the stable Ag_{Si}–V_C–V_{Si} cluster and is given below. However, the Ag_C–$2V_{Si}$ cluster will be considered as an activated state for the Ag_{Si}–V_C–V_{Si} cluster, effectively including its contribution to Ag diffusion.

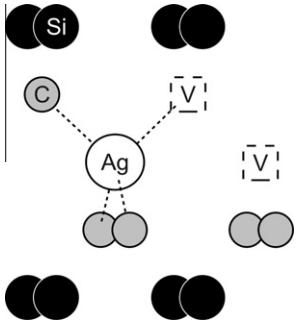

Fig. 4. Schematic picture of the unrelaxed Ag_{Si}–V_C–V_{Si} defect cluster.

The energies for Ag substitutionals with a vacancy as the next nearest neighbor on the same sub-lattice as the Ag are reported in Table 4 and are important for the analysis of substitutional diffusion. These are denoted at Ag_{Si}–V_{Si} and Ag_C–V_C. Both Ag_{Si}–V_{Si} and Ag_C–V_C are mechanically stable but energetically metastable, and under significant perturbations they collapse to more stable structures. Specifically, Ag_{Si}–V_{Si} is unstable with respect to the formation of Ag_{Si}–V_C–C_{Si} under all doping conditions, which implies that simple vacancy mediated impurity diffusion of Ag on the Si sub-lattice via direct hops to Si vacancies does not occur. When the Si vacancy approaches the Ag_{Si} defect, the C atom that is between the two falls into the Si vacancy, creating an antisite defect, and the Ag moves toward the vacant C site (similar to in the geometry of Ag_{Si}–V_C), as shown in Fig. 5. Similarly to Ag_{Si}–V_{Si}, the Ag_C–V_C defect is unstable to Ag_{Si}–V_C–Si_C (Fig. 6), although this is the case only under the n-type doping conditions. Also similarly to the Ag_{Si} case, this instability implies that simple vacancy mediated impurity diffusion of Ag on the C sub-lattice via direct hops to C vacancies does not occur in n-type doping conditions. Diffusion analysis is therefore not done for Ag substitutionals in this work. Instead, analysis of diffusion of Ag_{Si}–V_C–Si_C and Ag_{Si}–V_C–C_{Si} will be done and is given below.

3.3. Migration barriers

Migration barriers that are needed for a diffusion analysis of Ag in SiC are listed in Table 5. Barriers are calculated using the nudged elastic band (NEB) method with at least three images in each case unless otherwise noted. Barriers are determined for the most stable charge states under n-type doping. Barriers listed for point defects (vacancies, substitutionals, and interstitials) are those directly

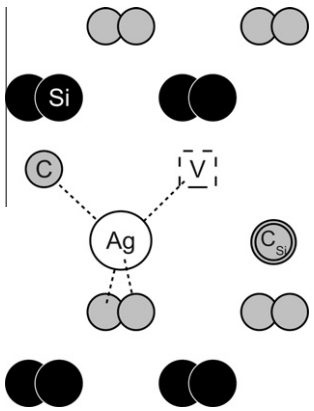

Fig. 5. Schematic picture of the Ag_{Si}–V_C–C_{Si} defect cluster.

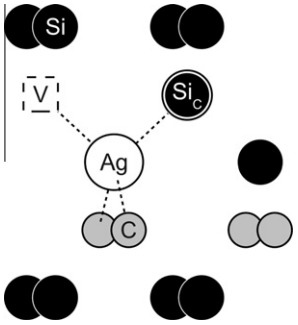

Fig. 6. Schematic picture of the Ag_{Si}–V_C–Si_C defect cluster.

Table 5
Migration energies for the most stable defects under n-type conditions. The multiple barriers listed for Si–Si $\langle 1\,1\,0\rangle^0$ and C–C $\langle 1\,0\,0\rangle^0$ correspond to different individual hops, as explained in the text. Some values for defect clusters are only lower bounds on the actual barrier. Please see the text for details.

Defect/reaction	Barrier (eV)
V_{Si}^{2-}	2.70
V_C^0	3.66
Si–Si $\langle 1\,1\,0\rangle^0$	1.48/0.83/1.13
C–C $\langle 1\,0\,0\rangle^0$	0.67/1.42
Ag_{TC}^0	0.89
Ag_{Si}–V_C^{-1}	9.10
Ag_{Si}–$2V_C^0$	$\geqslant$6.61
Ag_{Si}–V_C–V_{Si}^{4-}	5.49
Ag_{Si}–V_C–C_{Si}^{1-}	$\geqslant$6.25
Ag_{Si}–V_C–Si_C^{1-}	$\geqslant$5.60

calculated from the NEB calculation. Barriers listed for Ag defect clusters come from the analysis of several diffusion paths studied for each cluster. Each path is a series of hops that will be described in Section 4. For each path a rate-limiting barrier is determined, where the rate-limiting barrier is the change in energy from the starting point in the path to the maximum energy along the path. All the rate-limiting barriers are then compared among possible paths for a given cluster and the lowest one is reported in Table 5. It is assumed that diffusion of a cluster will be dominated by this rate-limiting barrier. A detailed example of this procedure for the Ag_{Si}–V_C defect cluster is presented in Section 4.3.

Table 5 also lists a number of barriers for self-interstitials. These are not used in the diffusion mechanisms discussed for Ag in this paper but we include a brief description of these energies for completeness. It should be noted that the migration energies given here are for elementary interstitial hops, which may lead to diffusion only in one direction or even not lead to long-range diffusion at all (e.g., due to caging effects).

In Table 5 the multiple barriers listed for the Si–Si $\langle 1\,1\,0\rangle^0$ dumbbell correspond to different single hops of the defect in the lattice. The first number is the barrier to move one of the Si atoms in a direction parallel to the dumbbell's direction. The second number is the barrier to move one of the Si atoms in a direction perpendicular to the dumbbell's direction, and is the smallest of the barriers investigated. The third number is the barrier to rotate the dumbbell around the $\langle 1\,0\,0\rangle$ axis.

Barriers listed for the C–C $\langle 1\,0\,0\rangle^0$ dumbbell, as with the Si dumbbell, are for different hops available to the defect. The first number is the barrier for a path that moves one of the C atoms through a C–Si $\langle 1\,0\,0\rangle$ configuration. This barrier is calculated to be 0.67 eV and is the lowest barrier investigated for the C–C $\langle 1\,0\,0\rangle$ split interstitial. The second number is the barrier to hop one of the C atoms through a path that does not bond the moving C to a Si atom, but instead moves the C atom directly to a neighboring C site. The barrier for this hop is 1.42 eV. The direction of this path is perpendicular to the first path. If the first hop were taken along the 110 direction, the second hop would be in the $1\bar{1}0$ direction.

The barrier to hop the Ag_{TC} interstitial is quite low as compared to moving substitutional Si, C, or Ag, suggesting that intrinsic diffusion of the Ag interstitials will be fast relative to substitutional diffusion. However, the high formation energy of the interstitials will inhibit their ability to transport Ag effectively. The implications of the migration and formation energetics for Ag transport are discussed in detail in the Section 4.

4. Discussion

4.1. Effective Ag diffusion

The effective diffusion coefficient for a given defect is composed of two parts, an intrinsic component and a concentration factor [46], and can be written as

$$D_{\text{def}}^{\text{eff}} = D_{\text{def}}^{\text{int}} \frac{c(\text{def})}{\text{sum of Ag defect concentrations}} \tag{2}$$

where $D_{\text{def}}^{\text{eff}}$ is the intrinsic diffusion coefficient for a defect and c(def) is the concentration of that defect. The intrinsic diffusion coefficient is the diffusivity of the defect assuming it exists 100% of the time. However, since Ag may spend only a fraction of its time as any specific type of defect, the effective diffusion coefficient for Ag in a given defect, $D_{\text{def}}^{\text{eff}}$, must be determined by modifying the $D_{\text{def}}^{\text{int}}$ by the fraction of time Ag is in that defect. The concentration ratio provides the necessary modification. Thus the diffusion coefficient for a given state of Ag will always be scaled by the fraction of time that Ag spends in that state. In the following all diffusion coefficients will be represented by an Arrhenius relation ($D = D_0\ \exp[-Q\beta]$), where $\beta = 1/(k_B T)$, D_0 is a constant prefactor, and Q is the activation energy of the diffusion mechanism. We will report the intrinsic and effective prefactors (D_0^{eff} and D_0^{eff}) and activation energies (Q^{int} and Q^{eff}); these results are summarized in Table 6. The Arrhenius representation is not rigorously exact but turns out to be a very good approximation for our models as linear fits of $\ln(D)$ vs. $1/T$ typically yield $R^2 = 1.00$ over the temperature range used for fitting. Therefore, for all the data reported in this section the fitting to an Arrhenius relation introduces no significant error into the calculated diffusion coefficients.

In the subsequent sections we will first calculate $D_{\text{def}}^{\text{int}}$ for each defect and then we will scale it by the appropriate concentration ratio, which will be determined from defect formation energies. The concentration of each defect type is approximately given by a constant prefactor and the Boltzmann factor of the defect formation energy. The prefactor will always cancel in application of Eq.

Table 6
Intrinsic and effective diffusion coefficients for Ag defects studied in this paper (values for n-type Si-rich conditions).

Defect	Q^{int} (eV)	D_0^{int} (m^2/s)	Q^{eff} (eV)	D_0^{eff} (m^2/s)
Ag_{TC}^0	0.89	9.57×10^{-8}	7.88	6.30×10^{-8}
Ag_{Si}–V_C^{1-}	9.10	9.57×10^{-8}	9.06	6.30×10^{-8}
Ag_{Si}–$2V_C^0$	$\geqslant$6.61	9.57×10^{-8}	$\geqslant$9.55	6.30×10^{-8}
Ag_{Si}–V_C–V_{Si}^{4-}	5.49	9.57×10^{-8}	8.65	6.30×10^{-8}
Ag_{Si}–V_C–C_{Si}^{1-}	$\geqslant$6.25	9.57×10^{-8}	$\geqslant$9.66	6.30×10^{-8}
Ag_{Si}–V_C–Si_C^{1-}	$\geqslant$5.60	9.57×10^{-8}	$\geqslant$7.91	6.30×10^{-8}

(2) so just the Boltzmann factors will be used to represent the concentrations. For example, if the only defects present in the system were Ag_{Si} and Ag_{Si}–V_C then the denominator in Eq. (2) would be $(\exp[-3.71\beta] + \exp[-3.46\beta])$. Contributions from all identified defects are included in the calculation of the denominator of Eq. (2). Below we describe the determination of the rate-limiting barrier and the estimation of D_{def}^{int} and D_{def}^{eff} for each of the Ag defects identified in this work. Calculations are carried out for n-type SiC and a Si-rich environment. As pointed out in Section 3.2, Ag substitutional diffusion analysis will not be done here as Ag_C–V_C and Ag_{Si}–V_{Si} are unstable structures.

4.2. Ag interstitials

The intrinsic diffusion coefficient $D_{Ag_{TC}}^{int}$ is given by $D_0^{int} \times \exp(-\beta Q^{int})$ where Q^{int} is equal to the migration barrier. For the Ag interstitial, the migration barrier is 0.89 eV. We will assume that D_0^{int} is the hop distance squared multiplied by an attempt frequency. This expression for D_0 does not include any effects of geometrical constraints on the allowed hop directions and does not account for the possibility of having more than one interstitial atom per lattice site. The hop distance is the same as the Si–Si or C–C distance in SiC, which is 3.09 Å. Assuming the attempt frequency to be equal to the phonon frequency of 10^{12} Hz, we estimate $D_0^{int} = 9.57 \times 10^{-8}$ m^2/s. Note that in the analysis of the prefactor we have neglected contributions from defect formation and migration entropies. These contributions typically contribute 1–2 orders of magnitude to D_0^{int}.

Inserting the intrinsic diffusion coefficient for Ag_{TC} and the concentration of Ag_{TC} $(\exp[-10.49\beta])$ into Eq. (2), the effective diffusion coefficient D^{eff} can be obtained as a function of T. Fitting this function to an Arrhenius relation in the range 800–1800 °C yields $D_0^{int} = 6.30 \times 10^{-8}$ m^2/s and Q^{eff} = 7.88 eV.

4.3. Ag_{Si}–V_C

Diffusion analysis for Ag defect clusters is more complicated than the analysis just done for Ag interstitials. The reason for this complexity is that there are many different ways of moving the defect cluster within the SiC lattice. Therefore, the following Sections 4.3–4.7 will contain detailed analysis of many diffusion pathways, many of which will turn out to be very slow and have little effect on Ag diffusion. The detailed analysis demonstrates that the search has been comprehensive and provides guidance for those interested in hopping mechanisms for defect clusters. However, if the reader is not interested in these details, they are invited to skip to Section 4.8 which provides a summary on the different mechanisms of Ag diffusion.

In order to make the analysis of defect cluster diffusion simpler, we will adhere to the following rules in considering what hops are possible for the defect cluster: (1) the accompanying defects (i.e., the defects that make up the cluster with Ag) must remain in either first nearest neighbor or second nearest neighbor configuration with the Ag and (2) Ag movement must hop directly to the accompanying defects or use the space provided by the accompanying defects to move. The reason for (1) is that if a defect in the defect cluster becomes separated beyond second nearest neighbor distance the diffusion analysis should be treated as diffusion without the accompanying defect because the accompanying defect is not able to enhance Ag movement when separated beyond that distance. At such large separations the defect cluster is treated as effectively having become unbound. For example, consider Ag_{Si}–V_C. If the accompanying V_C were to move beyond the second nearest neighbor shell of the Ag_{Si}, diffusion analysis should be done on Ag_{Si} alone without the aid of V_C. The V_C is unable to enhance Ag_{Si} diffusion unless it is close enough to Ag_{Si} to let the empty space provided by the vacancy help Ag move in the lattice. The reason for (2) is that we seek to understand how the accompanying defects help Ag movement. All defect clusters involve Ag_{Si} as one of the defects. If Ag moved in such a way as to not use space provided by the accompanying defects, the Ag would be swapping places with another Si atom in the close packed SiC structure. This puts two atoms into the same interstitial space, where that interstitial space is limited in size by the surrounding pure SiC lattice. Such movements are not energetically favorable. We will therefore restrict our analysis to Ag movements that involve using the defect cluster's accompanying defects.

In treating each defect cluster, we will be looking for paths where each path can be defined to be a series of atomic hops that move the defect cluster to a symmetrically equivalent configuration that is displaced from the initial configuration by the distance of second nearest neighbors in SiC (i.e., a path that hops Ag from one Si to another neighboring site). In looking at this definition of a path, it is helpful to realize that there are two types of hops: (1) hops that actually move Ag and (2) hops that just move the accompanying defects around Ag. Hops of type 2 generally have lower barriers and serve to change the orientation of the cluster. They are generally not rate-limiting barriers and will be called reorientation hops. Hops of type (1) actually move Ag and generally provide the rate-limiting barriers. These will be called Ag hops. Therefore, it is helpful to divide paths into two types of paths: (1) reorientation paths which are a series of reorientation hops and (2) Ag paths which are a series of Ag hops. In the following, reorientation paths will generally be presented first as they do not provide the rate-limiting barriers for the defect cluster's diffusion. After treating the reorientation paths, Ag paths will be treated to find their rate-limiting barriers which, in general, provide the rate-limiting barriers for the defect cluster's diffusion.

Note that in the following discussion of Ag_{Si}–V_C diffusion, all energies of activated states will be given relative to the energy of the Ag_{Si}–V_C cluster. This will be done even when the specific hop being considered is an intermediate along a multistep path, and therefore may not be a hop that starts from the Ag_{Si}–V_C cluster. Although this reference may be less intuitive in some cases, when referenced this way the largest activation energy can simply be taken as the rate-limiting barrier for the path under discussion.

The Ag_{Si}–V_C defect cluster has two methods of moving the accompanying defect V_C such that the V_C stays within the distance needed to aid Ag movement. Therefore, there are two reorientation paths:

i. The C vacancy hopping around the Ag_{Si} to another C lattice site (similar to normal C vacancy diffusion but with a Ag_{Si} as the nearest neighbor). There is only one reorientation hop in this reorientation path. The barrier for this hop was calculated to be 8.02 eV, which will also be the rate-limiting barrier for this reorientation path. While this barrier is quite high, it will be shown that Ag paths for this cluster will have higher rate-limiting barriers.
ii. The C vacancy hopping away from Ag as in Fig. 7a. The C vacancy is now unbound from the Ag atom. The C vacancy then hops as Fig. 7b to reform the defect cluster. There are two reorientation hops in this reorientation path that are actually equivalent and just mirror images of each other. The barrier for each of these hops, relative to the formation energy of Ag_{Si}–V_C, was calculated to be 5.97 eV, which is also the rate-limiting barrier for this reorientation path.

There are only two Ag hops available that utilize the V_C. The first is Ag moving into the C vacancy, and the other is the Ag swapping with a neighboring Si by moving through the space provided by the C vacancy. The former is a stable hop only if a Si atom fills the

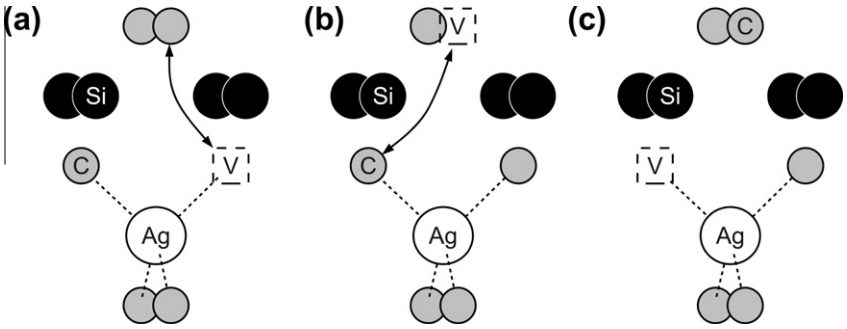

Fig. 7. Schematic picture showing a reorientation path of moving the C vacancy within the Ag_{Si}–V_C defect complex. (a) The initial configuration and the first reorientation hop where the C vacancy swaps places with a second nearest-neighbor C. (b) The intermediate configuration with C vacancy is unbound from Ag. (c) The final configuration after the C vacancy hops back toward Ag.

vacancy left behind by the Ag; otherwise, the Ag would fall back toward the Si site rather than stay near the C site. Therefore, there are only two Ag paths available:

i. A direct swapping of the Ag_{Si} with a neighboring Si, as depicted in Fig. 8. There is only one Ag hop in this Ag path. The barrier was calculated to be 9.10 eV and is the rate-limiting barrier for this Ag path.
ii. Ag_{Si} moving into the C vacancy while a Si simultaneously hops into the Si site that used to be occupied by the Ag atom, as shown in Fig. 9a. Ag occupies a C site, and the vacancy is on a Si site. Then, the Ag atom moves into a Si site at the same time the Si atom that occupies that site hops to fill the Si vacancy as depicted in Fig. 9b. There are two Ag hops in this Ag path that are actually equivalent and mirror images of each other. The barrier for both of these hops was calculated to be 9.21 eV and is the rate-limiting barrier for this Ag path.

The lowest rate-limiting barrier for the Ag paths was that for directly swapping the Ag with a neighboring Si, 9.10 eV. All of the rate-limiting barriers for the reorientation paths are lower than this value, therefore the rate-limiting barrier for Ag_{Si}–V_C diffusion is 9.10 eV, and the intrinsic diffusion activation energy Q^{int} is assumed to be equal to the rate-limiting barrier. The intrinsic prefactor D_0^{int} is taken to be the same as with Ag interstitials (9.57×10^{-8} m^2/s).

We stress again that all of these energies are reported relative to the formation energy of the starting configuration (Ag_{Si}–V_C). This approach is somewhat unconventional for hops that do not start from the Ag_{Si}–V_C state; however, it is justified here because it is the total change in energy from the stable cluster to the top of the barrier that controls diffusion.

Inserting the intrinsic diffusion coefficient for Ag_{Si}–V_C and the concentration of Ag_{Si}–V_C ($\exp[-3.46\beta]$) into Eq. (2), the effective diffusion coefficient D^{eff} can be obtained as a function of T. Fitting this function to an Arrhenius relation in the range of 800–1800 °C yields $D_0^{eff} = 6.30 \times 10^{-8}$ m^2/s and $Q^{eff} = 9.06$ eV.

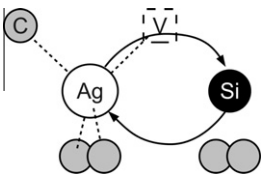

Fig. 8. Schematic picture of a simple Ag and Si hop in the Ag_{Si}–V_C defect cluster. The hopping path is shown by the arrows.

4.4. Ag_{Si}–$2V_C$

We will now analyze the larger Ag defect clusters. In these defect clusters, the Ag atom is accompanied by more than one additional defect, such as two C vacancies around a Ag on Si substitutional defect (Ag_{Si}–$2V_C$). In general, the diffusion of clusters is quite complex, and all possible paths cannot practically be explored with well converged *ab initio* elastic band calculations. Therefore, the goal of the following analysis will be to determine if any path might provide a faster diffusion mechanisms than interstitial Ag ($Q^{eff} = 7.88$ eV), which is the fastest diffusion mechanism for Ag we have found up to this point.

For the treatment of Ag_{Si}–$2V_C$ diffusion analysis, we will assume that the intrinsic prefactor D_0^{int} for all paths is equal to 9.57×10^{-8} m^2/s, which is the same as used for Ag interstitials. The Ag_{Si}–$2V_C$ defect cluster has only one reorientation path that consists of a single reorientation hop: moving a C vacancy around the Ag atom. The barrier for this reorientation path was found to be 5.02 eV. If this barrier were assumed to be Q^{int} for Ag_{Si}–$2V_C$, Eq. (2) predicts $Q^{eff} = 7.96$ eV, a value that is slightly larger than Q^{eff} for Ag interstitials (7.88 eV). To determine if the cluster has additional higher barriers it is necessary to consider the possible cluster hopping mechanisms. As the cluster hopping mechanisms can be quite complex and difficult to converge, the analysis below combines select calculations of key steps with more qualitative arguments.

To determine Ag paths, we first consider the three types of Ag hops in the Ag_{Si}–$2V_C$ cluster. Illustrations of these hops will be provided in the context of the Ag paths that comprise them. The first Ag hop moves Ag on the line defined by the two vacancies. The second Ag hop moves Ag through the two vacancies to another Si site. The third Ag hop moves the Ag atom into one of the C vacancies, but this configuration is unstable unless a neighboring Si moves into the Si site which used to hold the Ag. These combined hops effectively unbind both vacancies from the Ag and may be energetically unfavorable based upon the binding energy for Ag_{Si}–$2V_C$ (−5.66 eV). Ag hops of type three will not be explicitly investigated as it turns out to be a possible activated state for Ag paths that use Ag hops of type 2.

Three Ag paths can be constructed to investigate the remaining two Ag hops. The first identified Ag path is a ring diffusion mechanism based on the second Ag hop mentioned above and is schematically shown in Fig. 10. In this mechanism the Ag atom moves through one of the first nearest-neighbor C vacancies to one of the second nearest neighbor Si lattice sites. In this process Ag will kick out a Si atom, which in turn will move to another nearest neighbor Si site kicking out the second Si atom. The latter Si atom will move into the site that was originally occupied by the Ag atom. At the same time a C atom will move into the C vacancy from which the Ag atom moved away. A one-image nudged elastic

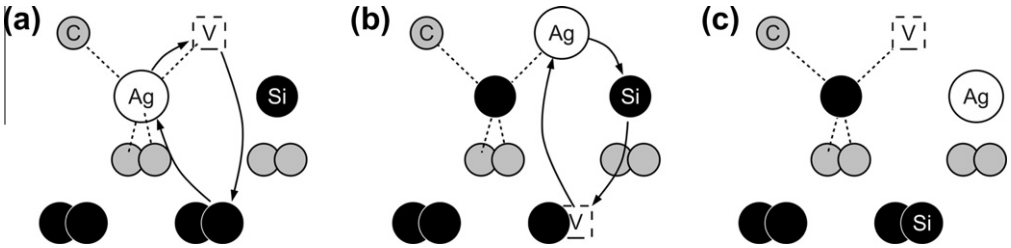

Fig. 9. Schematic picture of moving Ag in the Ag_{Si}–V_C defect cluster via an indirect Si hop. (a) The initial configuration along with hop paths. Ag moves to the C site, and Si vacancy hops away from Ag. (b) The intermediate configuration along with hop paths that bring Si vacancy back to Ag. (c) The final configuration.

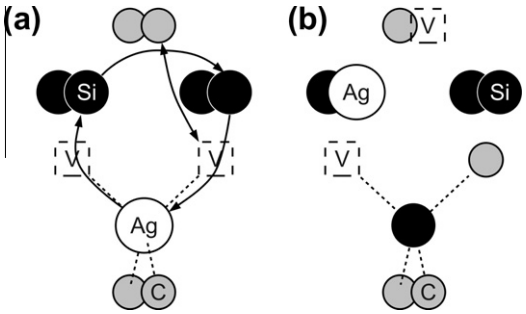

Fig. 10. Ring mechanism of diffusion for Ag_{Si}–$2V_C$. (a) Initial configuration of the defect cluster. Here, the Ag atom, two Si atoms, and a C atom move in a clockwise rotation to move the entire defect cluster. (b) Final configuration after all atoms move.

band (NEB) calculation of this hop yields a migration barrier of 6.61 eV relative to the formation energy of Ag_{Si}–$2V_C$. Although more images are required in NEB calculations to determine the barrier accurately, the estimated 6.61 eV can be considered as a lower bound on the actual barrier. If we assume Q^{int} for Ag_{Si}–$2V_C$ is equal to 6.61 eV, Eq. (2) predicts Q^{eff} for Ag_{Si}–$2V_C$ to be 9.55 eV. As Q^{eff} for Ag interstitials is 7.88 eV, this first Ag path for Ag_{Si}–$2V_C$ will diffuse Ag far slower than the Ag interstitial mechanism.

The second possible Ag path for Ag_{Si}–$2V_C$ is shown in Fig. 11 and is based on the second Ag hop described above. In the first step the Ag atom switches positions with a Si atom utilizing the space provided by the two nearby C vacancies (Fig. 11a). In this process one of the C vacancies is unbound from Ag in that it no longer tetrahedrally coordinates the Ag atom (Fig. 11b). A C atom that does tetrahedrally-coordinate the Ag's new position then hops into the unbound C vacancy (Fig. 11b); this effectively rebinds the C vacancy to the Ag atom (Fig. 11c). A one-image NEB calculation gives the barrier of the first step in this path (Fig. 11a) to be 7.04 eV relative to the formation energy of Ag_{Si}–$2V_C$. Similarly to the hops considered in the second path and discussed in previous paragraphs, here the migration barrier is not exact, but rather it provides a lower bound on the actual barrier. This estimated barrier for diffusion of the Ag_{Si}–$2V_C$ defect complex is larger than the barrier obtained for the first Ag path, and will therefore be slower than that mechanism. The second Ag path will not be considered further.

The third and last Ag path we considered is similar to the second path in that one of the C vacancies is unbound from the Ag atom, but it is based on the first Ag hop described above. As shown in Fig. 12a this process is accomplished in such a way as to use the space of only one of the C vacancies to switch the Ag atom with a neighboring Si atom. This swapping of Ag and Si positions is the first step in this path. In the second step, the unbound C vacancy will have to hop around the lattice to rebind to the Ag atom (Fig. 12b). Two different possibilities exist for the C vacancy movement and are shown in Fig. 12b.

An estimate of the barrier for the first step in this Ag path can be obtained by an analysis of similar hops that have already been investigated. The second Ag path for Ag_{Si}–$2V_C$ involves Ag swapping with Si by using two C vacancies (Fig. 11a). The barrier for that Ag hop was calculated to be at least 7.04 eV. In the investigation of Ag_{Si}–V_C, two methods of swapping Ag with a neighboring Si using the bound C vacancy were considered (Figs. 8 and 9). Each had a barrier over 9 eV. These high barriers from previous calculations suggest that the barrier for swapping Ag with Si in the third Ag path for Ag_{Si}–$2V_C$ (Fig. 11a) will also be high. It is not unreasonable to expect the barrier for this Ag–Si swap to be over 7 eV. Thus, the rate-limiting barrier for the third Ag path will be at least as large as the barrier found for the second Ag path investigated for Ag_{Si}–$2V_C$. As the second Ag path has already been established as slow compared to the first Ag path, we will not consider Ag path three further.

To summarize the above discussion, we found that the lowest barrier found for the Ag_{Si}–$2V_C$ defect cluster to be at least

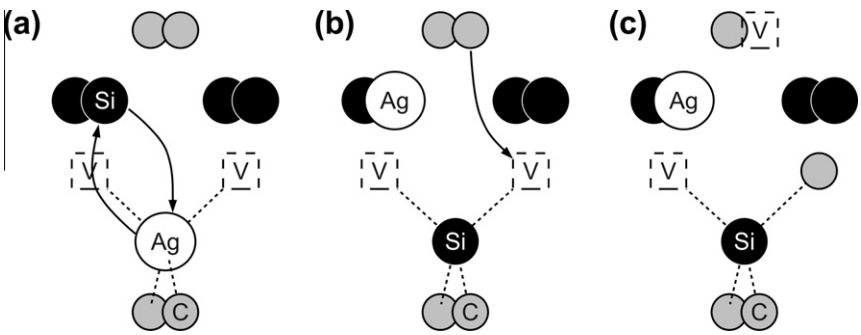

Fig. 11. Hopping mechanism for Ag_{Si}–$2V_C$ where one of the vacancies is unbound by the switching of the Ag with a Si atom. The space of both C vacancies is available for this hop. The initial configuration and the hopping path are shown in (a). In part (b), a C atom is shown to hop into the unbound C vacancy. The final configuration of the defect cluster is shown in (c).

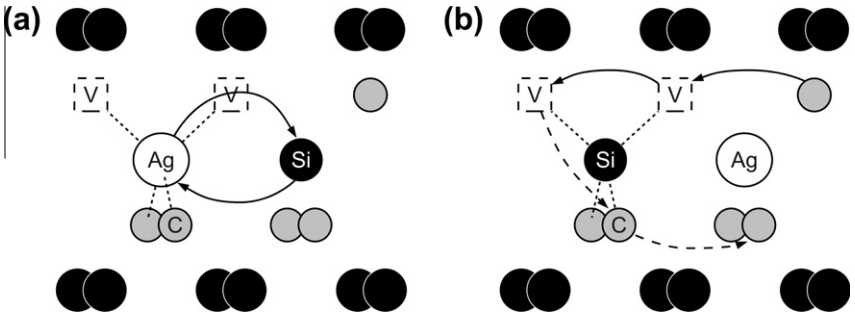

Fig. 12. Hopping mechanism for Ag_{Si}–$2V_C$ where the space of only one C vacancy is used for the Ag–Si swap. The initial configuration and the Ag–Si swap are depicted in (a). Part (b) shows the intermediate configuration and possible pathways to rebind the unbound C vacancy. Two possible paths exist for the unbound C vacancy: a C moves via two hops directly through the vacancies (solid arrows), or the C vacancy hops around the C sub-lattice until it reaches a C site next to the Ag atom (dashed arrows).

6.61 eV. This predicts a Q^{eff} for the Ag_{Si}–$2V_C$ cluster to be greater than 9.55 eV which is larger than that of Ag interstitials (7.88 eV).

4.5. Ag_{Si}–V_C–V_{Si}

For the treatment of reorientation and Ag paths in the Ag_{Si}–V_C–V_{Si} defect cluster, we deviate from the procedure used in previous defect clusters and will first present the Ag paths rather than the orientation paths as it turns out that moving Ag in Ag_{Si}–V_C–V_{Si} is very easy and does not provide the rate-limiting barriers for Ag_{Si}–V_C–V_{Si} diffusion.

There are three possible Ag paths. They are shown in Fig. 13. Each Ag path has only one Ag hop:

i. Ag swaps with the V_{Si}; shown by the solid line in Fig. 13. This is an easy hop that has a barrier of 0.58 eV. This low barrier for the Ag–V_{Si} swap implies that Ag can move freely between the Si sites in this defect cluster. The activated state for this path is the Ag_C–$2V_{Si}$ defect cluster.
ii. Ag moves into the V_C; shown by the dashed-dotted line in Fig. 13. The only way for this to be stable, however, is for two Si atoms to fill the two Si vacancies at the same time; otherwise the Ag atom will quickly fall back onto a Si site. This type of movement (two Si atoms moving to fill the two vacancies at the same time) is not likely. The Ag–V_{Si} swap in (i) above already provides a ready mechanism to move Ag. As it is unlikely for this new Ag path to have a lower barrier this Ag path is not considered further.
iii. Ag swaps with a Si atom that tetrahehrally coordinates the V_C; shown by the dashed line in Fig. 13. This type of movement only utilizes the space of the V_C and puts two atoms within that interstitial space. Such a process has not yielded a low barrier in similar hops investigated for other defect clusters (see Ag_{Si}–V_C and Ag_{Si}–$2V_C$). This hop, and therefore this Ag path, is unlikely to have a lower barrier than that found for the Ag–V_{Si} swap. This path will not be considered further.

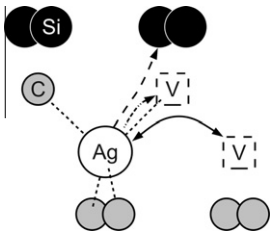

Fig. 13. Possible hops for Ag in Ag_{Si}–V_C–V_{Si}.

Due to the expectation that others barriers will be higher, the only barrier investigated with *ab initio* is that for the first Ag path (i), which swaps Ag with the V_{Si}. As this barrier is so low, it is unlikely that another Ag path exists that will be faster, and if one does exist, it will have a small impact on the overall diffusivity of Ag_{Si}–V_C–V_{Si}. The rate-limiting barrier for the Ag paths is therefore set at the barrier for path (i) above, or 0.58 eV.

There are two reorientation paths that include four unique reorientation hops available to the Ag_{Si}–V_C–V_{Si} structure:

i. V_{Si} hops around V_C as shown in Fig. 14a. The Si vacancy then hops away from the C vacancy (Fig. 14b) and the Si vacancy is now unbound from the cluster. In the next step (Fig. 14c), the C vacancy hops to reform the defect cluster. The final configuration of the defect cluster is shown in Fig. 14d. There are three distinct reorientation hops in this path. The last two hops can actually proceed in any order.
ii. The C vacancy hops around Ag (Fig. 15a) in such a way that the Si vacancy must hop at least twice to reform the cluster. One possibility for the Si hop is via the solid line in Fig. 15b and then via the dashed line in the same figure, where the latter hop reforms the cluster. Alternatively, the Si vacancy can hop via the dashed-dotted line in Fig. 15b, but this configuration is indistinguishable in terms of energy and symmetry from the configuration before the Si vacancy hop. Consequently the two other hops (solid and dashed lines) for the Si vacancy are still necessary to reform the cluster. There are three distinct reorientation hops in this reorientation path. The last V_{Si} hop (the hop that ultimately reforms the cluster), the dashed line in Fig. 15b, is the reverse of the second V_{Si} hop in path (i) and therefore has the same barrier.

The first reorientation hop for the first reorientation path has a calculated barrier of 2.45 eV. The second reorientation hop, that of the V_{Si} hopping away from the V_C (shown in Fig. 14b), has a calculated barrier of 3.63 eV. The third hop (Fig. 14c), which is the C vacancy hop, can actually proceed either by a direct hop (solid arrow) or by an indirect hop (dashed arrows) where the C vacancy hops away from the Ag and then back to it. The indirect type of reorientation hops are also seen in the analysis of Ag_{Si}–V_C in Section 4.3. The barrier to hop the C atom directly to the neighboring C lattice site is 5.49 eV. The barrier to hop the C vacancy away from Ag is calculated to be 4.06 eV and the barrier to hop it back is 5.84 eV. The rate-limiting barrier for the indirect hop is 5.84 eV which is higher than the 5.49 barrier for directly hopping the C vacancy (Fig. 14c solid arrow). Therefore we will assume the third reorientation hop in the first reorientation path proceeds with the C vacancy hopping directly around the Ag atom and has a barrier of

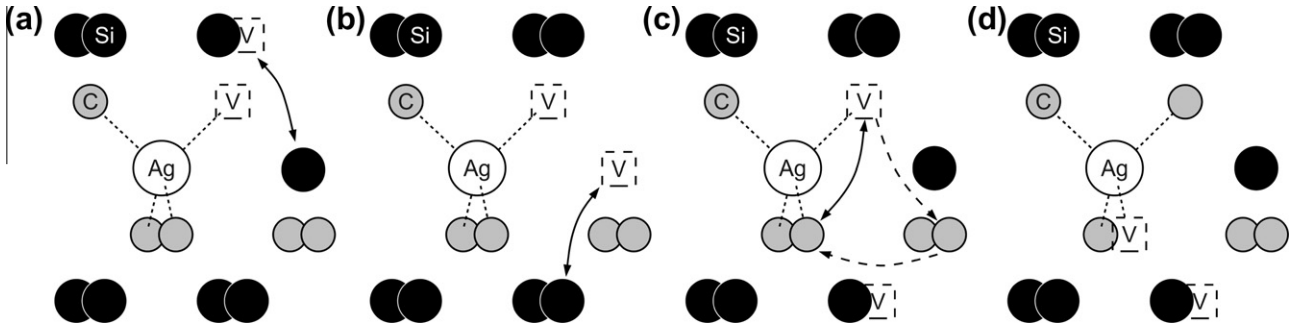

Fig. 14. A reorientation path for Ag_{Si}–V_C–V_{Si}. The initial configuration is shown in (a) where the Si vacancy will then hop around the C vacancy. In (b) the Si vacancy hops away from the C vacancy which then follows the Si vacancy by hopping as shown in (c). The final configuration of the defect cluster is shown in (d).

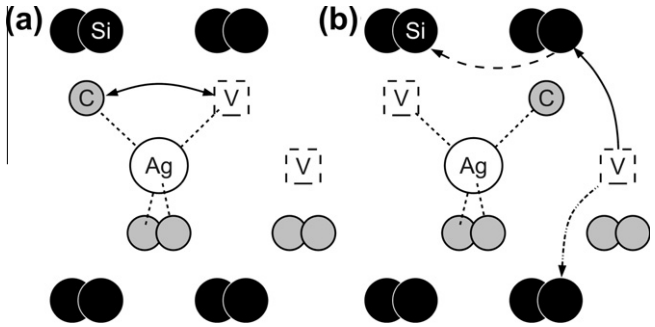

Fig. 15. Depiction of the second reorientation path for Ag_{Si}–V_C–V_{Si}. The C vacancy hops away from the Si vacancy so that the Si vacancy must hop at least twice to reform the cluster. In part (a), the C vacancy hops away. In (b) the Si vacancy can move to reform the defect cluster by two possible paths: the first is a path of two hops depicted by the solid and dashed lines, the second is a path that hops the Si vacancy around the Si lattice, depicted by the dashed-dotted line.

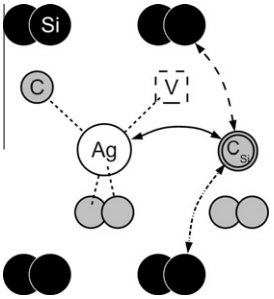

Fig. 16. Possible hops for C_{Si} in Ag_{Si}–V_C–C_{Si}. Details provided in text.

5.49 eV. The rate-limiting barrier for reorientation path one is 5.49 eV.

In the second reorientation path, the first reorientation hop (Fig. 15a) has a barrier of at least 7.02 eV as predicted by a one-image NEB calculation. Since this barrier is already larger than that calculated for the first reorientation path, we will not calculate barriers for the remaining reorientation hops nor an intrinsic diffusion constant for the second reorientation path.

Based on the rate-limiting barrier for reorientation path 1, the intrinsic diffusion coefficient Q^{int} for Ag_{Si}–V_C–V_{Si} is estimated to be 5.49 eV. Similarly to the other hopping species the intrinsic prefactor D_0^{int} is assumed to be 9.57×10^{-8} m^2/s (see discussion of Ag interstitial diffusion for the derivation).

Inserting the intrinsic diffusion coefficient for Ag_{Si}–V_C–V_{Si} and the concentration of Ag_{Si}–V_C–V_{Si} ($\exp[-6.65\beta]$) into Eq. (2), the effective diffusion coefficient D^{eff} can be obtained as a function of T. Fitting this function to an Arrhenius relation in the range of 800–1800 °C yields $D_0^{eff} = 6.30 \times 10^{-8}$ m^2/s and $Q^{eff} = 8.65$ eV.

4.6. Ag_{Si}–V_C–C_{Si}

The Ag_{Si}–V_C–C_{Si} defect cluster is similar in configuration to Ag_{Si}–V_C–V_{Si} except that the V_{Si} becomes a C_{Si}. Here, it will be shown that investigation of how the C_{Si} can move is all that is necessary to show that this defect cluster will have a larger Q^{eff} than interstitial diffusion. If all the barriers to move C_{Si} predict slower Q^{eff} than interstitial diffusion, it will not be necessary to construct and investigate diffusion paths for Ag_{Si}–V_C–C_{Si} as all paths will include at least one hop to move C_{Si}.

We identify three key hops of the C_{Si} that control the diffusion of the Ag_{Si}–V_C–C_{Si} cluster. These hops are all depicted in Fig. 16. There are two reorientation hops and one Ag hop. The hops depicted by the dashed line and the dashed-dotted line are reorientation hops. The first reorientation hop has C_{Si} switching places with a Si atom that tetrahedrally coordinates the C vacancy (dashed line in Fig. 16). The migration barrier for this swap is 7.35 eV. The second reorientation hop (dashed-dotted line in Fig. 16) moves the antisite defect away from the C vacancy. Using one-image NEB calculations we predict this hop to have a barrier of at least 9.14 eV. The Ag hop is marked with the solid line in Fig. 16; the C_{Si} can swap with Ag. This hop is particularly important as other hops for the Ag atom are expected to be very high based on our earlier analysis of the Ag_{Si}–V_C cluster. The activated state for this hop is also the same activated state for Ag simple diffusion on the Si sub-lattice; therefore, simple Si substitutional diffusion is directly considered via the analysis of this hop. The barrier for swapping of Ag and C_{Si} is calculated to be 6.25 eV. The high barriers for hopping C_{Si} are not that surprising given that all the hops involve two atoms being in the same interstitial space at the same time. Since hopping of C_{Si} by one of these three hops is necessary to diffuse the Ag_{Si}–V_C–V_{Si} cluster, we can conclude that the intrinsic activation barrier Q^{int} for Ag_{Si}–V_C–C_{Si} is at least 6.25 eV, the smallest of the investigated barriers. Using the same intrinsic prefactor D_0^{int} as for other defect clusters (9.57×10^{-8} m^2/s) Eq. (2) predicts Q^{eff} will be at least 9.66 eV for the Ag_{Si}–V_C–C_{Si} defect cluster. As this Q^{eff} is larger than that for Ag interstitials, no other hops need to be investigated for this cluster.

4.7. Ag_{Si}–V_C–Si_C

The Ag_{Si}–V_C–V_{Si} defect is similar in structure to Ag_{Si}–$2V_C$. As with Ag_{Si}–V_C–C_{Si} we only need to consider the reorientation hops associated with Si_C movement in the Ag_{Si}–V_C–Si_C cluster to determine the diffusivity of the Ag_{Si}–V_C–Si_C defect cluster. There are two possible reorientation hops for Si_C and are depicted in Fig. 17.

The first reorientation hop involves moving the Si_C to another C site that is occupied by a C atom (the dashed line in Fig. 17). The

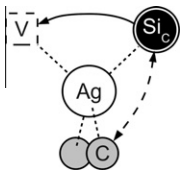

Fig. 17. Possible hops for Si_C that re-orient the Ag_{Si}–V_C–Si_C defect cluster.

barrier for this reorientation hop is 6.27 eV. The second reorientation hop moves the Si_C to the existing C vacancy (the solid line in Fig. 17). The barrier for this reorientation hop is 5.60 eV. As reorientation hops of these two types must be present to effectively move the defect cluster, we conclude that intrinsic activation barrier Q^{int} for Ag_{Si}–V_C–Si_C will be at least 5.6 eV. Assuming D_0^{int} is the same as for other defect clusters (9.57×10^{-8} m^2/s), Q^{eff} is at least 7.91 eV according to Eq. (2). Therefore, at best, Ag_{Si}–V_C–Si_C will move Ag slightly slower than the Ag interstitial mechanism. Given the high barriers obtained for Ag movement in the Ag_{Si}–V_C defect cluster, it is likely that Q^{int} is larger than 5.60 eV for Ag_{Si}–V_C–Si_C. A high barrier to move Ag would potentially make Ag_{Si}–V_C–Si_C diffusion much slower than Ag interstitial diffusion. However, a detailed study of Ag path barriers has not been undertaken on this cluster.

4.8. Summary

All the diffusion coefficients, both intrinsic and effective, that were discussed in this paper are summarized in Table 6. Our results predict that in single-crystal SiC Ag will diffuse primarily as an interstitial, with an effective activation barrier of 7.88 eV. Although the intrinsic diffusion barrier for Ag interstitial diffusion is only 0.89 eV, the effective diffusion rate is significantly reduced by the relatively short time Ag spends as an interstitial. This reduction is the result of the high formation energies of Ag interstitials.

As shown in Table 1, the experimentally determined upper bounds for the Ag diffusion coefficient in bulk SiC are 5×10^{-21} m^2/s (1500 °C) [8] and 10^{-21} m^2/s (1300 °C) [7]. Using the Ag interstitial D_0^{eff} and Q^{eff} from Table 6, we estimate the diffusion coefficient of Ag at 1300 °C and 1500 °C to be 3.6×10^{-33} and 2.5×10^{-30} m^2/s, respectively. These predicted diffusion coefficients are well below the upper bounds proposed for Ag bulk diffusion, and are thus consistent with the existing understanding that Ag bulk diffusion is very slow and is not able to account for the relatively fast diffusion seen in integral release measurements on polycrystalline SiC. If one assumes that the measured diffusion coefficients from polycrystalline samples (see Table 1) are due to grain boundary diffusion, then the very low bulk diffusivity predicted in our study is consistent with Ag in SiC having type C kinetics [47].

The key energies for Ag diffusion in bulk SiC can be identified from the data presented here. The most stable Ag defects in the system, which consist of Ag defect clusters, are characterized by large migration energies. Ag is therefore effectively trapped in the substitutional and cluster defects. The fastest mechanism, the interstitial mechanism, is hard for Ag to access due to the high formation energies for Ag interstitials. While the Ag atom can diffuse quite fast as an interstitial, it is only able to do so rarely.

The identification of these key energies, high migration barriers for defect clusters and high formation energy for Ag interstitials, will allow us to focus investigations on diffusion in more complex structures, such as grain boundaries. If it is easier to move defect clusters in grain boundary structures, Ag diffusion will be enhanced, as the majority of Ag in the system (assuming significant grain boundary segregation) will be able to move more freely. If it becomes easier to form Ag interstitials in grain boundaries, Ag will be able to more readily access the faster interstitial diffusion mechanism, which will also enhance overall Ag diffusion.

As all the results here have been presented for n-type Si-rich conditions, it is important to consider how the diffusion coefficients may change under different external chemical potentials of Si, C and electrons. First, we consider changing from Si-rich to C-rich conditions. In C-rich conditions, C based defects (V_C, Ag_C, Ag_{Si}–$2V_C$) will change their formation energy in the positive direction (toward being less stable) by the calculated heat of formation of SiC (−0.44 eV), which will reduce their effective diffusion coefficients by making the defects less prevalent. Si based defects (V_{Si}, Ag_{Si}, Ag_C–$2V_{Si}$) would change their formation energy in the negative direction (toward being more stable) by the same amount, thus speeding up their effective diffusion. Ag_{Si} would become the dominant defect in n-type C-rich conditions (as opposed to Ag_{Si}–V_C, which is most stable under Si-rich conditions). Intrinsic diffusion coefficients for all defects studied here would remain the same, as they do not depend on the formation energy of any other defect. Under n-type C-rich conditions we predict Ag_{TC} to be still the fastest diffuser with effective activation energy of 8.07 eV and an effective prefactor of 5.93×10^{-8} m^2/s. These values are quite close to those found under Si-rich conditions, suggesting that no dramatic change in diffusivity is associated with a change from a Si- to C-rich environment.

According to Fig. 1, the most dominant defects in Si-rich and p-type doping conditions will be Ag on C substitutionals with a charge state of 3+. C-rich conditions will not change this ordering although the formation energies for both Ag_C and Ag_{Si}–$2V_C$ will increase while the formation energy for Ag_{Si}–V_C will remain the same. Ag on C substitutional diffusion will be possible given that Ag_C–V_C is stable in the p-type doping limit. On the other hand Ag on Si substitutional diffusion will not be favorable because Ag_{Si}–V_{Si} is still metastable with respect to Ag_{Si}–V_C–C_{Si}. It is expected that the diffusion coefficient for Ag_C in C-rich conditions will be slower than in Si-rich conditions due to the higher formation energy for C vacancies in the C-rich limit. The concentration ratio in Eq. (2) will be dominated by the concentration of Ag on C substitutionals. Diffusion coefficients for p-type conditions could be determined by the same approach as taken in this work for n-type conditions. However, barriers would have to be calculated for the charge states that are stable in p-type conditions which has not been attempted in this paper.

5. Conclusions

Using *ab initio* calculations, we have determined the structures and charge states of intrinsic and Ag defects in bulk cubic 3C–SiC (also called β-SiC) as well as the mechanisms of Ag diffusion in this material. Our calculations have been carried out using the proper formalism for open systems, which includes dependence of formation and migration energies on the external chemical potentials of Si, C and electrons. Charged defect calculations are corrected to the extent possible for errors arising from core electronic alignment, electrostatic interactions, and under-estimation of the band gap. All charged defect calculations have been checked to ensure that charge states do reside in the gap. Diffusion analysis has focused on n-type Si-rich SiC, which is consistent with the doping of as-prepared SiC. However, the data and approaches presented here provide a foundation for further analysis of defects in other environments that correspond to different external chemical potentials.

We considered possible Ag defect structures consisting of Ag_C and Ag_{Si} substitutionals, Ag interstitials, and Ag-vacancy defect complexes. We determined that Ag will most likely be found in

the defect cluster consisting of Ag on a Si sub-lattice site coupled with a C vacancy with a charge state of $1-\left(Ag_{Si}-V_C^{1-}\right)$.

The fastest diffusion mechanism for Ag in bulk SiC was found to be that of Ag interstitials with an effective activation energy of 7.88 eV and an effective prefactor of $6.30\times10^{-8}\,m^2/s$. This diffusion coefficient is consistent with upper bounds of Ag diffusion in bulk SiC proposed in the literature, and implies that Ag is not likely to be transported by bulk diffusion. Bulk diffusion is limited by high migration barriers for the most stable Ag defects and the inability of Ag to reach the faster diffusing interstitial state due to the high formation energy of interstitials. Other mechanisms, such as grain boundary diffusion, must be investigated in order to account for the amount of Ag transport seen in integral release and polycrystalline ion-implantation experiments.

Acknowledgements

This work is supported by the DoE NERI Grant Award No. DE-FC07-07ID14823 and computing support from the National Science Foundation (NSF) National Center for Supercomputing Applications (NCSA), Award No. DMR060007.

References

[1] D.P. Petti, TRISO-Coated Particle Fuel Phenomenon Identification and Ranking Tables (PIRTs) for Fission Product Transport Due to Manufacturing Operations, and Accidents, in, US, Nuclear Regulatory Commission, Washington, DC, 2004 (20555-0001).
[2] Fuel Performance and Fission Product Behavior in Gas Cooled Reactors, IAEA-TECDOC-978, 1997.
[3] H. Nabielek, SiC for fuel, in: 33rd ICACCS Discussion Group of Symposium 10 on silicon carbide, Daytona Beach, FL, 2009.
[4] H. Nabielek, P.E. Brown, P. Offerman, Nucl. Technol. 35 (1977) 483–493.
[5] K. Verfondern, R.C. Martin, R. Moormann, Methods and data for HTGR fuel performance and radionuclide release modeling during normal operation and accidents for safety analyses, Jül-2721 Forschungszentrum Jülich GmbH, January 1993.
[6] W. Amian, D. Stover, Nucl. Technol. 61 (1983) 475–486.
[7] E. Friedland, J.B. Malherbe, N.G. van der Berg, T. Hlatshwayo, A.J. Botha, E. Wendler, W. Wesch, J. Nucl. Mater. 389 (2009) 326–331.
[8] H.J. MacLean, Silver Transport in CVD Silicon Carbide, PhD Thesis, Department of Nuclear Engineering, MIT, Boston, 2004.
[9] T.J. Gerczak, T.R. Allen, Z. Zhu, Fission Product Transport of Cesium and Silver in CVD-SiC, in: Embedded Topical on Nuclear Fuels and Structural Materials for the Next Generation Nuclear Reactors, ANS Annual Meeting, San Diego, CA, USA, 2010.
[10] P.E. Blöchl, Phys. Rev. B 50 (1994) 17953.
[11] G. Kresse, D. Joubert, Phys. Rev. B 59 (1999) 1758.
[12] G. Kresse, J. Furthmüller, Comput. Mater. Sci. 6 (1996) 15.
[13] G. Kresse, J. Furthmüller, Phys. Rev. B 54 (1996) 11169.
[14] G. Kresse, J. Hafner, Phys. Rev. B 47 (1993) 558.
[15] G. Kresse, J. Hafner, Phys. Rev. B 49 (1994) 14251.
[16] J.P. Perdew, K. Burke, M. Ernzerhof, Phys. Rev. Lett. 77 (1996) 3865.
[17] J.P. Perdew, K. Burke, M. Ernzerhof, Phys. Rev. Lett. 78 (1997) 1396.
[18] A.F. Kohan, G. Ceder, D. Morgan, C.G. Van de Walle, Phys. Rev. B 61 (2000) 15019–15027.
[19] J. Li, S.H. Wei, S.S. Li, J.B. Xia, Phys. Rev. B 74 (2006) 081201.
[20] S. Lany, A. Zunger, Phys. Rev. B 78 (2008) 235104.
[21] M. Bockstedte, A. Mattausch, O. Pankratov, Phys. Rev. B 68 (2003) 205201.
[22] G. Makov, M.C. Payne, Phys. Rev. B 51 (1995) 4014–4022.
[23] C.G. Van de Walle, J. Neugebauer, J. Appl. Phys. 95 (2004) 3851–3879.
[24] G. Kresse, M. Marsman, J. Furthmuller, VASP the GUIDE <http://cms.mpi.univie.ac.at/vasp> (accessed 12.05.10).
[25] W.J. Choyke, D.R. Hamilton, L. Patrick, Phys. Rev. 133 (1964) A1163.
[26] P. Erhart, K. Albe, A. Klein, Phys. Rev. B 73 (2006) 205203.
[27] A. Janotti, C.G. Van de Walle, Phys. Rev. B 76 (2007) 165202.
[28] C.W.M. Castleton, A. Hoglund, S. Mirbt, Modell. Simul. Mater. Sci. Eng. 17 (2009) 21.
[29] A. Alkauskas, P. Broqvist, A. Pasquarello, Phys. Rev. Lett. 101 (2008) 046405.
[30] S.J. Clark, J. Robertson, S. Lany, A. Zunger, Phys. Rev. B 81 (2010) 115311.
[31] S. Lany, A. Zunger, Phys. Rev. B 81 (2010) 113201.
[32] P. Rinke, A. Janotti, M. Scheffler, C.G. Van de Walle, Phys. Rev. Lett. 102 (2009) 026402.
[33] A. Zywietz, J. Furthmuller, F. Bechstedt, Phys. Rev. B 59 (1999) 15166–15180.
[34] J.B. Casady, R.W. Johnson, Solid State Electron. 39 (1996) 1409–1422.
[35] C. Wang, J. Bernholc, R.F. Davis, Phys. Rev. B 38 (1988) 12752–12755.
[36] H.J. Kim, R.F. Davis, J. Electrochem. Soc. 133 (1986) 2350–2357.
[37] T. Tachibana, H.S. Kong, Y.C. Wang, R.F. Davis, J. Appl. Phys. 67 (1990) 6375–6381.
[38] R.M. Van Ginhoven, A. Chartier, C. Meis, W.J. Weber, L.R. Corrales, J. Nucl. Mater. 348 (2006) 51–59.
[39] L. Torpo, T.E.M. Staab, R.M. Nieminen, Phys. Rev. B 65 (2002) 085202.
[40] B. Aradi, A. Gali, P. Deák, J.E. Lowther, N.T. Son, E. Janzén, W.J. Choyke, Phys. Rev. B 63 (2001) 245202.
[41] F. Gao, E.J. Bylaska, W.J. Weber, L.R. Corrales, Nucl. Instrum. Methods Phys. Res. B 180 (2001) 286–292.
[42] A. Mattausch, M. Bockstedte, O. Pankratov, Physica B 308 (2001) 656–659.
[43] M. Posselt, F. Gao, W.J. Weber, V. Belko, J. Phys. Condens. Matter 16 (2004) 1307–1323.
[44] David R. Lide, CRC Handbook of Chemistry and Physics (Internet Version 2010), 90th ed., CRC Press/Taylor and Francis, Boca Raton, FL, 2010.
[45] L. Pauling, The Nature of the Chemical Bond, Cornell University Press, Ithica, NY, 1939.
[46] R.J. Borg, G.J. Dienes, An Introduction to Solid State Diffusion, Academic Press, Inc., 1988. pp. 93–96.
[47] L.G. Harrison, Trans. Farady Soc. (1961) 1191.